Hetero-Bimetallic Paddlewheel Complexes for Enhanced CO_2 Reduction Selectivity: A First Principles Study

Journal:	*Physical Chemistry Chemical Physics*
Manuscript ID	CP-ART-11-2023-005694.R1
Article Type:	Paper
Date Submitted by the Author:	26-Jan-2024
Complete List of Authors:	McCarver, Gavin; National Institute of Standards and Technology, NIST Center for Neutron Research Yildirim, Taner; National Institute of Standards and Technology, NIST Center for Neutron Research Zhou, Wei; National Institute of Standards and Technology, NIST Center for Neutron Research

Journal Name

ARTICLE TYPE

Cite this: DOI: 00.0000/xxxxxxxxxx

Hetero-Bimetallic Paddlewheel Complexes for Enhanced CO_2 Reduction Selectivity in MOFs: A First Principles Study[†]

Gavin A. McCarver,* Taner Yildirim, and Wei Zhou

Received Date
Accepted Date

DOI: 00.0000/xxxxxxxxxx

The reduction of carbon dioxide (CO_2) into value-added feedstock materials, fine chemicals, and fuels represents a crucial approach for meeting contemporary chemical demands while reducing dependence on petrochemical sources. Optimizing catalysts for the CO_2 reduction reaction (CO_2RR) can entail employing first principles methodology to identify catalysts possessing desirable attributes, including the ability to form diverse products or selectively produce a limited set of products, or exhibit favorable reaction kinetics. In this study, we investigate CO_2RR on bimetallic Cu-based paddlewheel complexes, aiming to understand the impact metal substitution with Mn(II), Co(II), or Ni(II) has on bimetallic paddlewheel metal-organic frameworks. Substituting one of the Cu sites of the paddlewheel complex with Mn results in a more catalytically active Cu center, poised to produce substantial quantities of formic acid (HCOOH) and smaller quantities of methane (CH_4) with a suppressed production of C_2 products such as ethanol (CH_3CH_2OH) or ethylene (C_2H_4). Moreover, the presence of Mn significantly reduces the limiting potential for CO_2 reduction from 2.22 eV on the homo-bimetallic Cu paddlewheel complex to 1.19 eV, thereby necessitating a smaller applied potential. Conversely, within the Co-substituted paddlewheel complex, the Co site emerges as the primary catalytic center, selectively yielding CH_4 as the sole reduced CO_2 product, with a limiting potential of 1.22 eV. Notably, the Co site faces significant competition from H_2 production due to a lower limiting potential of 0.81 eV for hydrogen reduction. Our examination of the Cu-Ni paddlewheel complex, featuring a Ni substituent site, reveals two catalytically active centers, each promoting distinct reductive processes. Both the Ni and Cu sites exhibit a propensity for HCOOH formation, with the Ni site favoring further reduction to CH_4, whereas the Cu site directs the reaction towards methanol (CH_3OH) production. This study holds significance in informing and streamlining future experimental efforts for synthesizing and evaluating novel catalysts with superior capabilities for CO_2 reduction.

1 Introduction

The increasing utilization of petroleum-based fuels has contributed to a persistent and growing accumulation of greenhouse gases, notably CO_2, in the Earth's atmosphere.[1–3] This surge has led to adverse consequences such as rising global temperatures, increased air pollution, and intensified extreme weather events. To mitigate this upward trend, an array of technologies collectively known as carbon capture, utilization, and sequestration (CCUS) are being developed to reduce levels of atmospheric CO_2.[4] This entails capturing CO_2 emissions and subsequently employing them for immediate utilization or long-term storage. The process of CO_2 utilization involves its conversion into value-added materials, including various fuels (e.g., methane, methanol), fine chemicals (e.g., formaldehyde, formic acid), and feedstock materials (e.g., ethylene), thus serving as a sustainable alternative to petroleum-based resources.[5]

Several methodologies, including thermal hydrogenation[6–8] and (photo)electrochemical reduction,[9,10] are currently under investigation for the activation and utilization of CO_2. Electrochemical reduction, in particular, offers a distinctive approach by allowing precise control over product formation through voltage modulation.[11] Notably, Kuhl and colleagues[12] have exemplified this phenomenon during CO_2 reduction on metallic copper surfaces. Their investigation revealed up to fifteen distinct CO_2 reduction products, whose composition significantly varied with applied voltage. At lower voltages (-0.9 V vs. RHE), the predominant products included CH_4, formate, CO, C_2H_4, and H_2, while higher voltages led to the formation of C_3 products like n-propanol or acetone in addition to other C_1 and C_2 products.

National Institute of Standards and Technology, Center for Neutron Research, Gaithersburg, Maryland 20899-6102, United States; E-mail: gavin.mccarver@nist.gov

[†] Electronic Supplementary Information (ESI) available: [details of any supplementary information available should be included here]. See DOI: 00.0000/00000000.

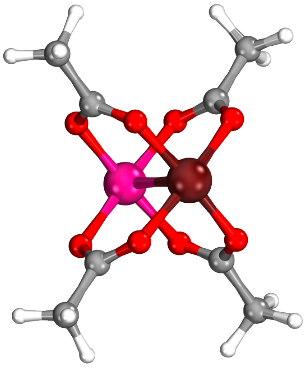

Fig. 1 Model paddlewheel complex used to study the CO_2 reduction reaction on HKUST-1. Color code: H (white), C (grey), O (red), Cu (brown), substituent metal (pink).

In contrast to metallic surfaces, materials such as metal organic frameworks (MOFs) offer highly dispersed and well-defined active sites that bridge the gap between traditional heterogeneous and homogeneous catalysis.[13] However, most MOFs are electrical insulators, which historically posed challenges for electrochemical studies and CO_2 reduction. Nevertheless, recent research has demonstrated that even insulating MOFs can serve as effective electrocatalysts for CO_2 reduction.[14–24] Building upon the seminal work of Weng *et al.*[14] who demonstrated that HKUST-1 could effectively reduce CO_2 to CH_4, research by Nam *et al.*[15] and Perfecto-Irigaray *et al.*[16] explored how the effects of structural distortions on HKUST-1 MOFs, yielding diverse CO_2 reduction products. Nam and colleagues induced MOF distortion through thermal treatments, achieving higher C_2H_4 production with a remarkable Faradaic efficiency (FE) of 45% for MOF-derived Cu cluster catalysts. Conversely, Perfecto-Irigaray *et al.* introduced metal dopants (Zn(II), Ru(III), or Pd(II)) to induce distortions to HKUST-1. They observed changes in the FE of CH_3CH_2OH and CH_3OH production. However, their work revealed that a stable FE plateau was eventually reached, similar to or lower than that of the unsubstituted MOF, irrespective of the dopant metal.

Improving upon the findings of Perfecto-Irigaray *et al.* and Nam *et al.*, our study takes a significant step forward by employing first principles methods to investigate the thermodynamics of CO_2 reduction on hetero-bimetallic paddlewheel cluster models of the substituted HKUST-1 MOF (Figure 1). In contrast to previous research, we explore the substituent metals Mn(II), Co(II), and Ni(II), as these metals are expected to modify the electronic structure of the adjacent Cu site while providing an alternative active site for catalysis. Importantly, our choice of Mn(II),[25–27] Co(II),[26–30] and Ni(II)[26,28] as substituents is supported by experimental evidence demonstrating the incorporation of these metals into the HKUST-1 framework through post-synthetic modification. This experimental validation reinforces our computational models' relevance and feasibility. While we initially considered including a Fe metal node,[31] we encountered challenges related to significant spin contamination, which could introduce potential inaccuracies into our energy calculations. Therefore, we opted to focus exclusively on the Mn, Co, and Ni substituent metals.

Our research reveals that substitution with Mn significantly reduces the energy barrier for the initial CO_2 reduction from 2.22 eV to 1.19 eV, resulting in enhanced production of HCOOH and complete suppression of C_2 product formation. In contrast, the Co site in the Co-substituted paddlewheel cluster exhibits stronger CO_2 adsorption and selective CH_4 production. However, this site also promotes more favorable hydrogen reduction to form H_2, potentially limiting CO_2 reduction efficiency. Lastly, Ni substitution results in both Ni and Cu sites with distinct reaction mechanisms, favoring HCOOH and CH_4 formation on the Ni site, while the Cu site predominantly produces HCOOH and CH_3OH. Our findings underscore the pivotal role of judicious metal substituent selection in HKUST-1, leading to significant modifications in product identity and proportions during CO_2 reduction.

2 Computational Details

To investigate the behavior of bimetallic paddlewheel MOFs, we used a truncated model of the open-metal site within the HKUST-1 MOF, which consisted of four acetate linkers and two metal nodes (Figure 1). While this cluster model can be used to describe many properties of paddlewheel MOFs, it fails to account for confinement effects that would be felt due to the porous nature of the MOF. Such models have previously proven effective in examining various aspects of HKUST-1 behavior, including reaction energetics.[6,28,32–34] In our study, we substituted one of the metal nodes with either Mn, Co, or Ni to investigate their influence on the CO_2 reduction reaction.

In an effort to preserve some of the inherent rigidity of the MOF material, we constrained the positions of the C atoms of the acetate linkers to their crystallographic positions, allowing all other atoms to fully relaxed during the optimization steps.[6,32] We conducted all calculations using the M06L[35] density functional as implemented in the ORCA 5.0.3[36] software package. For basis sets, we employed def2-TZVPP for the metal atoms, def2-TZVP for the first coordination sphere around the metal atoms and the adsorbate molecules, and def2-SV(P) for all other atoms.[37] The resolution of identity (RI)[38] method was utilized to accelerate the computation of all four-index integrals, employing the def2/J auxiliary basis set.[39] An unrestricted Khon-Sham wavefunction was assumed for all calculations and tight criteria were used for both the SCF and geometry optimization steps. To account for dispersion effects beyond those inherent in the MO6L density functional, we used the D3zero[40] method. Analytical frequency calculations were performed to ensure each structure corresponds to a local minimum and to derive thermodynamic quantities such as those shown in Eq. 1 using the quasi-rigid rotor harmonic oscillator (Qausi-RRHO) approximation.[41] Implicit solvation effects were considered using the continuum-like polarizable conductor model (CPCM), with H_2O as the solvent of choice.[42]

The total free energy (G) of each reactant, intermediate, and product was determined following Eq. 1, where E represents the total electronic energy and I encompasses the internal energy, accounting for zero-point energy and thermal effects. H and S denote enthalpic and entropic contributions, respectively, evaluated at T = 298K. Additionally, eU signifies the effect of an applied potential (U) per electron (e). We considered each elementary step of the reduction reaction to proceed through a

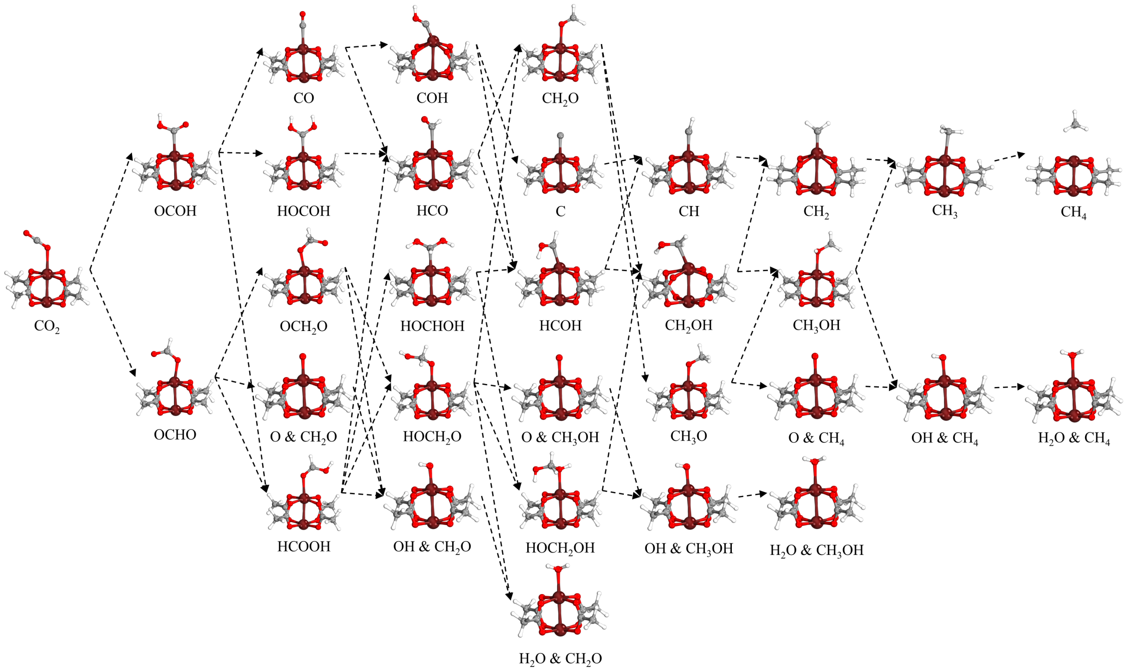

Fig. 2 C_1 reduction intermediates on the Cu-Cu paddlewheel complex. Arrows correspond to a reduction (PCET) step. Color code: H (white), C (grey), O (red), Cu (brown).

proton-coupled electron transfer (PCET) mechanism[43,44], entailing the addition of a hydrogen atom as a H^+/e^- pair to the system. This mechanism ensures the overall charge of the system is conserved throughout the reaction. The electrochemical reaction energies were referenced relative to the reactants, which included the paddlewheel complex, a CO_2 molecule, and H^+/e^- pairs representing the PCET steps. The energy of a single H^+/e^- pair is set to 1/2 H_2 following the computational hydrogen electrode (CHE) model.[11,45] We employed the CHE model as an initial approximation to elucidate the thermodynamics governing the CO_2 reduction mechanism. The limiting potential (U_L) was calculated based on the maximum difference (ΔG_{max}) between elementary reduction steps leading to the formation of a specific product.

$$G = E + I + H - TS - eU \tag{1}$$

3 Results & Discussion

3.1 Electronic Structure of substituted Paddlewheel Complexes

The relatively short inter-metallic distances inherent to the paddlewheel complexes often give rise to complex electronic structures. An illustrative example is observed in the Cu-Cu paddlewheel complex. Here, an antiferromagnetically coupled singlet ground spin state emerges as a consequence of the antiparallel spins on the Cu sites.[46] Consequently, a comprehensive understanding of the electronic structure of the substituted paddlewheel complexes is imperative for an insightful examination of the CO_2 reduction reaction. To determine the ground spin state of each paddlewheel complex, we examined both ferromagnetic and antiferromagnetic spin states with varying spin multiplicities (Table S2). During our examination, we observed variations in the structure of the paddlewheel complexes (Table S3).

For the Cu-Mn paddlewheel complex, we considered both a ferromagnetic septet and antiferromagnetically coupled quintet spin state (see Table S2 for spin populations). These states correspond to parallel and antiparallel spins between the two centers, with five unpaired electrons on the Mn site (S = 5/2) and one unpaired electron on the Cu site (S = 1/2). We considered only the possibility of a spin flip on the Cu site for the quintet state as the half-filled nature of the d-orbitals on the Mn site would preclude an energetically favorable intermediate spin state. The energy difference between these states was determined to be 2.7 kcal mol^{-1}, slightly smaller than the energy difference calculated between the antiferromagnetically coupled singlet and ferromagnetic triplet states of the Cu-Cu paddlewheel complex (2.9 kcal mol^{-1}). Consequently, we anticipate that the CO_2 reduction reaction will predominantly occur on the quintet spin state.

In the case of the Cu-Co paddlewheel complex, we examined four distinct spin states: ferromagnetic quintet and triplet spin states, as well as antiferromagnetically coupled triplet and singlet spin states. These states arise from the possibility of high spin (S = 3/2) and low spin (S = 1/2) states on the Co site, along with the prospect of a spin flip occurring on the Cu site. The ferromagnetic triplet spin state emerged as the ground spin state, characterized by parallel spins of S = 1/2 on the Co and Cu sites. The next highest spin state is the antiferromagnetically coupled singlet, lying 1.1 kcal mol^{-1} above in energy, and corresponding to the two sites having antiparallel, S = 1/2 and S = -1/2 spins. The small energy difference between these two states indicates an easy ability of the Cu site to switch between spin states, potentially affecting the catalytic activity of the center. Lastly, the ground spin state of the Cu-Ni paddlewheel complex was determined to be a ferromagnetic doublet, with an S = 0 Ni site.

3.2 CO_2 Reduction on the Cu-Cu Paddlewheel Complex

To elucidate how metal substituents influence Cu-paddlewheel complexes in the context of the CO_2 reduction reaction, we begin by conducting an in-depth analysis of the reaction on the Cu-Cu paddlewheel complex. As previously mentioned, Nam *et al.* [15] conducted studies that underscored the capacity of both Cu-acetate (CuAc) and HKUST-1 to mediate the reduction of CO_2 to products such as CO and C_2H_4. In our present study, we have elected to employ an acetate paddlewheel complex to model the open-metal sites of HKUST-1. This choice is anticipated to yield slight variations, akin to those observed by Nam *et al.*, between the two materials. However, our primary goal is to explore the potential of alternative metal substituents, which were not investigated by Perfecto-Irigaray *et al.*, in enhancing the CO_2 reduction reaction. Additionally, we constrained the positions of the C atoms in the paddlewheel complex to better approximate the rigidity of the MOF material using the paddlewheel model.

The initial step of CO_2 reduction on the Cu-Cu paddlewheel complex (Figure 2, 3) results in the formation of one of two intermediates: *OCHO for reduction at the C atom of CO_2 and *OCOH for the reduction at one of the O atoms. Here, the * symbol indicates the surface adsorption of the intermediate. The *OCHO and *OCOH intermediates exhibit comparable formation energies of 2.22 eV and 2.34 eV, respectively. The modest difference of 0.12 eV (2.8 kcal mol^{-1}) between their formation energies suggests that both intermediates should form with a slightly higher likelihood of the *OCHO intermediate forming. Subsequently, the *OCHO intermediate can undergo further reduction to form either *HCOOH or *O and CH_2O (formaldehyde), while the *OCOH intermediate can lead to the formation of *HCOOH, *CO, or *HOCOH. In either case, the closed-shell species (*CO and *HCOOH) are more energetically favored over the open-shell species (*HOCOH and *O). The *HCOOH intermediate exhibits slightly stronger binding to the Cu site compared to *CO, although both are weakly bound (Table S1), potentially explaining the formation of both formate and CO observed by Nam *et al.* with more CO being formed due to weaker binding.

Further reduction of both *CO and *HCOOH results in the favorable formation of *HCO with formation energies of 1.31 eV and 1.63 eV, respectively. While several other intermediates are possible, they lie higher in energy and are less likely to form. Subsequent reduction steps favor the formation of the closed-shell $^*CH_2O$ species over the open-shell *HCOH species by 1.81 eV, limiting the likelihood of its formation. Following this, both $^*CH_3O$ and $^*CH_2OH$ intermediates are expected to form due to their similar formation energies (1.19 eV and 1.12 eV, respectively), but both ultimately lead to the formation of $^*CH_3OH$ in subsequent steps. The reduction process then favors the formation of the *OH intermediate, accompanied by the release of free CH_4, culminating in the formation of an adsorbed $^*H_2O$ species as the final reduced intermediate. The strong binding of both the $^*CH_2O$ and $^*CH_3OH$ intermediates to the Cu site may explain their absence in the work of Nam *et al.* Consequently, our results suggest that the primary C_1 products of CO_2 reduction on the Cu-Cu paddlewheel complex are formic acid, carbon monoxide, and methane.

Both Nam *et al.* and Perfecto Irigaray *et al.* observed the production of C_2 products, namely C_2H_4, CH_3CH_2OH, and CH_3COOH (acetic acid), during CO_2 reduction. The formation of C_2 products results from the coupling of less strongly bound C_1 products on the catalyst surface. In the case of the Cu-Cu paddlewheel complex, intermediates that may lead to the formation of ethylene, ethanol, and acetic acid encompass *OCOH and $^*CH_2OH$ (Figure 2). CO-CO coupling was also considered, but we were unable to find a stable intermediate. These C_1 intermediates do not directly lead to the formation of the C_2 products, but instead require subsequent reduction: two equivalents of $^*CH_2OH$ followed by two reduction steps can lead to both ethanol (Eq. 2) and ethylene (Eq. 3) formation, while the coupling of $^*CH_2OH$ and *OCOH followed by two reduction steps, may result in the formation of acetic acid (Eq. 4).

$$\begin{aligned} 2CH_2OH \rightarrow (^*CH_2OH)_2 &\xrightarrow{H^+/e^-} \\ {}^*CH_2CH_2OH + H_2O &\xrightarrow{H^+/e^-} \\ {}^*CH_3CH_2OH + H_2O& \end{aligned} \tag{2}$$

$$\begin{aligned} 2CH_2OH \rightarrow (^*CH_2OH)_2 &\xrightarrow{H^+/e^-} \\ {}^*CH_2CH_2OH + H_2O &\xrightarrow{H^+/e^-} \\ {}^*C_2H_4 + 2H_2O& \end{aligned} \tag{3}$$

$$\begin{aligned} OCOH + CH_2OH \rightarrow {}^*HOCH_2CO_2H &\xrightarrow{H^+/e^-} \\ {}^*CH_2COOH + H_2O &\xrightarrow{H^+/e^-} \\ {}^*CH_3COOH + H_2O& \end{aligned} \tag{4}$$

The precursor for the formation of ethanol and ethylene is $(CH_2OH)_2$ (ethylene glycol), while the precursor for acetic acid is $HOCH_2CO_2H$ (glycolic acid). The formation of these precursors is both thermodynamically and electrochemically favorable due to two high-energy, open-shell intermediates coupling to form a lower-energy, closed-shell intermediate. The reduction of glycolic acid favors the formation of the $^*CH_2COOH$ and *OH intermediates, featuring small formation energies of 0.74 eV and 0.87 eV, respectively. The formation of the *OH intermediate coincides with the production of free CH_3COOH and necessitates subsequent reduction to yield $^*H_2O$, while the $^*CH_2COOH$ intermediate requires the further reduction of the methylene C to yield $^*CH_3COOH$, both processes being energetically favorable. Similarly, the initial reduction of $(CH_2OH)_2$ leads to the formation of $^*CH_2CH_2OH$ with a formation energy of 0.82 eV, which can be further reduced to either $^*C_2H_4$ and $^*CH_3CH_2OH$. $^*C_2H_4$ is formed upon the reduction of the O atom of $^*CH_2CH_2OH$, while $^*CH_3CH_2OH$ is formed following the reduction of the methylene C atom. Both of these reduction steps are energetically favorable, with a 0.15 eV (3.5 kcal mol^{-1}) difference, indicating the likelihood of both C_2H_4 and CH_3CH_2OH formation on the Cu-Cu

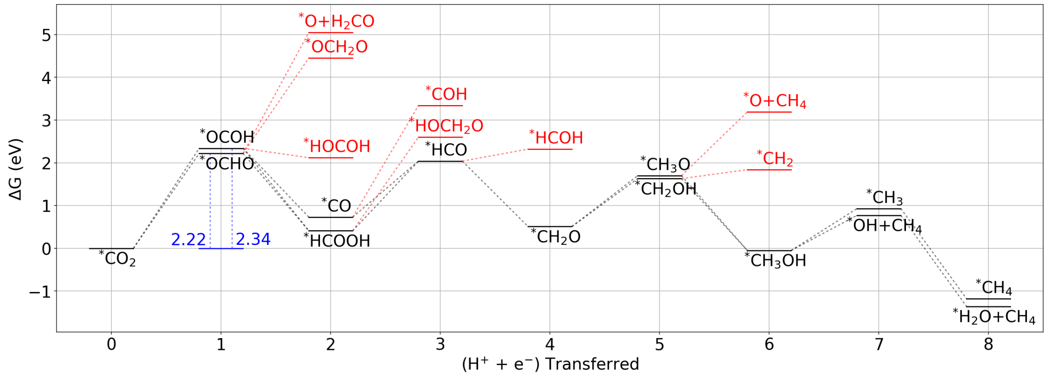

Fig. 3 Free energy reaction mechanism for the reduction of CO_2 on the Cu-Cu paddlewheel complex. Competing intermediates shown in red. Limiting potential values shown in blue and given in eV.

paddlewheel complex.

We also performed calculations using a Cu-Zn paddlewheel complex based upon the work of Perfecto-Irigaray *et al.*[16] who showed that doping HKUST-1 with Zn led to only minor modifications in the FE of CH_3CH_2OH production. The introduction of the Zn site changed the electronic structure of the Cu site only modestly, lowering the limiting potential for HCOOH by only 0.05 eV (Figure S1). Additionally, the reduction of CO_2 on the Zn site leads to a reaction pathway that is nearly identical to that of the unsubstituted, Cu-Cu paddlewheel complex (Figure S2). The largest difference is observed as a stronger binding of H_2O following CH_4 formation. The strong binding of H_2O competes with CO_2 adsorption for the Zn site and the minor change in the electronic structure of the Cu site are both expected to lead to only minor modification in the reduction of CO_2, as observed by Perfecto-Irigaray *et al.*.

Expanding on this analysis, we aim to elucidate how the introduction of Mn(II), Co(II), or Ni(II) as substituent metals to the Cu-Cu paddlewheel complex influences CO_2 reduction. We will emphasize the changes in the electronic structure of the Cu(II) site induced by the substituent metal and how that affects the CO_2 reduction reaction, as well as how CO_2 reduction proceeds on the substituent metal site.

3.3 Cu-Mn Paddlewheel Complex

Our investigations revealed significant electronic structure variations in the substituted paddlewheel complexes, with perhaps the largest impact observed when Mn is introduced. This variation arises from the distinct electronic configurations of the Mn and Cu sites. The Mn site favors a high spin d^5 configuration characterized by half-filled d-orbitals, whereas the Cu site can only accommodate a single unpaired electron due to its d^9 configuration. These significant variations in the electronic structures of the metal sites are reflected in the binding energy of CO_2, with a substantial 0.38 eV difference between them. Significantly, the Mn site exhibits a stronger interaction with CO_2, rendering it more favorable for CO_2 reduction.

Furthermore, we observed similar trends in other paddlewheel complexes. Sites most akin to the d^9 Cu site, such as d^8 Ni and d^{10} Zn, exhibited the smallest differences in CO_2 binding energy (0.10 and 0.05 eV, respectively). In the Cu-Co paddlewheel complex, a difference of 0.29 eV in CO_2 binding was observed, aligning more closely with the Cu-Mn complex than with either the Cu-Ni or Cu-Zn complexes. These findings emphasize the critical role of electronic structure variations in influencing the adsorption behavior of CO_2 on different metal sites within the paddlewheel complexes.

During the initial reduction of CO_2 (top of Figure 4), the formation of *OCHO is strongly favored over *OCOH, with a notable energy difference of 1.11 eV, limiting the formation of *OCOH and, consequently, *CO. Similar to the Cu-Cu paddlewheel complex, closed-shell intermediates are more favored here, resulting in the formation of *HCOOH over *O (and CH_2O) or $^*OCH_2O$. The energy required for the formation of *HCOOH on the Mn site is relatively low at 0.61 eV, indicating that only a small applied voltage would be required to reduce CO_2 to HCOOH. Nevertheless, the strong binding of *HCOOH on the Mn site implies limited desorption.

Subsequent reduction of *HCOOH can yield four different intermediates (*HOCHOH, $^*HOCH_2O$, *HCO, and *OH to form free CH_2O), with the formation of the Mn-OH moiety being the most favored. The *OH intermediate then requires a final reduction step to yield $^*H_2O$ and the already free CH_2O. The limiting potential for the formation of H_2O and CH_2O is 0.95 eV, higher than that of HCOOH formation, implying the need for a higher applied voltage for further *HCOOH reduction. It is expected that the Mn site favors the interaction with $^*H_2O$ rather than CH_2O due to the stronger binding energy (0.50 eV and 0.32 eV, respectively). This process ultimately results in the production of CH_2O and H_2O. However, the strong binding of H_2O suggests limited catalytic activity due to significant competition with CO_2.

In contrast to the Cu-Cu paddlewheel complex, the initial CO_2 reduction on the Cu site of the Cu-Mn paddlewheel complex strongly favors the formation of *OCHO over *OCOH by 0.80 eV. This inhibits *CO formation while favoring *HCOOH formation following a second reduction step (bottom of Figure 4). The *HCOOH intermediate can then undergo a subsequent reduction to lead to the *HCO and $^*HOCH_2O$ intermediates with similar formation energies of 1.19 eV and 1.16 eV, respectively. The small energy difference between these intermediates (0.03 eV,

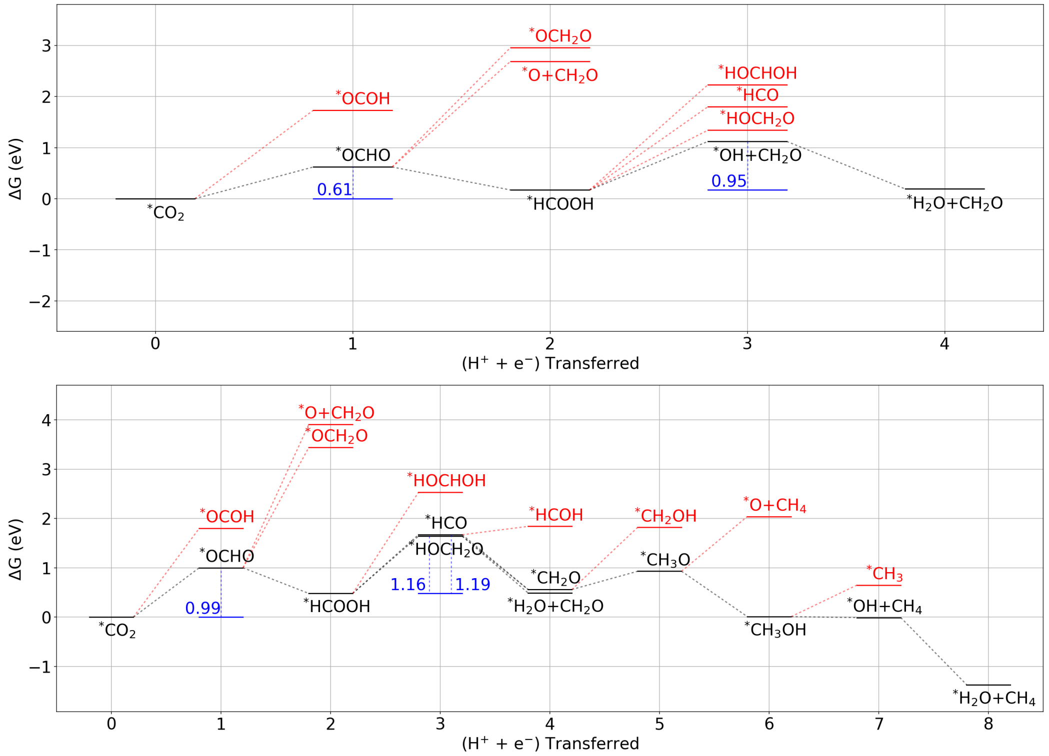

Fig. 4 Free energy reaction mechanism for the reduction of CO_2 on the Mn (top) and Cu (bottom) sites of the Cu-Mn paddlewheel complex. Competing intermediates shown in red. Limiting potential values shown in blue and given in eV.

0.8 kcal mol^{-1}) indicates comparable likelihoods of formation. The reduction of *HCO leads to several intermediates, including *CH_2O, *CH_3O, and *CH_3OH, without competition from other lower-lying intermediates forming. The reduction of the C atom of *CH_3OH is more favorable than the O atom, yielding *OH and free CH_4. The energy difference between these two reductions is 0.66 eV. *OH is then reduced to H_2O, yielding one equivalent of CH_4 and two equivalents of H_2O from the *HCO intermediate.

While the *HCO intermediate is expected to be reduced to only *CH_2O, with no H_2O evolved during this step, the *$HOCH_2O$ intermediate can be reduced to produce either *H_2O or *CH_2O. Both *H_2O and *CH_2O result in similar formation energies from *$HOCH_2O$ and similar binding energies to the Cu site (Table S1). These observations indicate that the reduction of *$HOCH_2O$ can lead to either free CH_2O or H_2O with similar likelihoods. If H_2O is produced and *CH_2O is bound to the surface, it suggests the reduction process may continue, ultimately leading to the formation of CH_4. However, if *H_2O remains adsorbed to the Cu site, subsequent reduction is unlikely to occur

The production of CH_4 from CO_2 reduction is contingent upon the effective binding of all intermediates to the Cu site, which may not occur in the case of the Cu-Mn paddlewheel complex. Weak binding of closed-shell intermediates at the Cu site implies a reduced likelihood of subsequent reduction steps as the reaction progresses. Consequently, we anticipate a predominant proportion of HCOOH, with only limited, if any, production of CH_2O, CH_3OH, or CH_4. This expectation contrasts with the findings of Nam *et al.*, who reported formate as a minor product from CO_2 reduction with HKUST-1. Additionally, few C_2 products are expected due to the favorable desorption of HCOOH which hinders the coupling of C_1 intermediates. Nevertheless, our results emphasize the substantial influence of the Mn site on modulating the CO_2 reduction reaction in the paddlewheel complexes.

3.4 Cu-Co Paddlewheel Complex

CO_2 exhibits a stronger interaction with the Co site of the Cu-Co paddlewheel complex, similar to the Cu-Mn paddlewheel complex. The difference in binding energy between the Cu and Co centers is slightly smaller at 0.29 eV. However, it remains substantial enough to strongly favor interaction with the Co site. In contrast to both the Cu-Cu and Cu-Mn complexes, the Co site of the Cu-Co paddlewheel complex exhibits a preference for the reduction of CO_2 to *OCOH over *OCHO, with a notable energy difference of 0.44 eV (Figure 5). The formation energy of *OCOH is 1.21 eV, considerably higher than that of hydrogen reduction on the site, which stands at 0.81 eV. This suggests that the reduction of CO_2 on the Co site may face strong competition from hydrogen reduction.

Nevertheless, the subsequent reduction of *OCOH favors the formation of both *CO and *HCOOH with similar formation energies. Subsequent reductions then yield *HCO, *CH_2O, *CH_3O, and *CH_3OH, following a pattern identical to that observed on the Cu site of the Cu-Mn paddlewheel complex. Each of the intermediates strongly interacts with the Co site, influencing two aspects of the reduction reaction: limiting the desorption of closed-shell intermediates and inhibiting the coupling of open-shell interme-

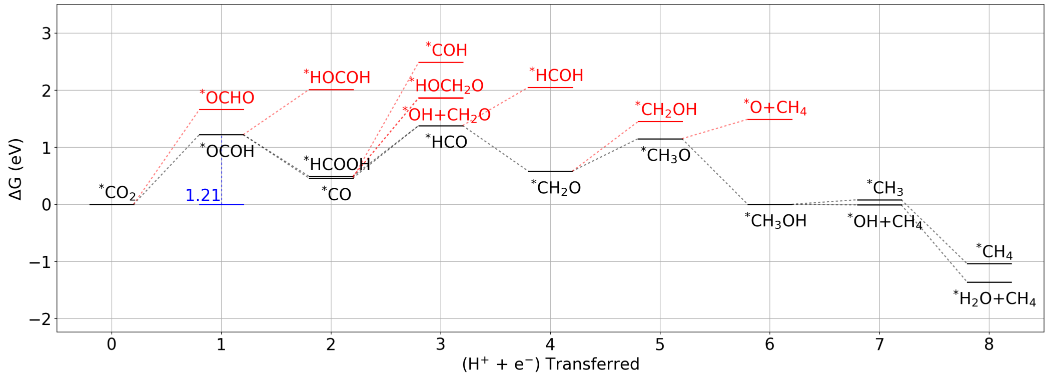

Fig. 5 Free energy reaction mechanism for the reduction of CO_2 on the Co site of the Cu-Co paddlewheel complex. Competing intermediates shown in red. Limiting potential values shown in blue and given in eV.

diates to form C_2 products.

Further reduction of $^*CH_3OH$ at both the C and O atoms lead to the formation of the $^*OH$ and $^*CH_3$ intermediates with similar formation energies. While the formation of the $^*OH$ intermediate is more favorable, both pathways ultimately result in the formation of CH_4—either adsorbed following the reduction of $^*CH_3$ or as a free gaseous product following the formation of $^*OH$. The strong binding of intermediates to the Co site is expected to then lead to the selective reduction of CO_2 to CH_4, in contrast to the sites of both the Cu-Mn and Cu-Cu paddlewheel complexes. Furthermore, H_2O exhibits weaker binding to the Co site compared to the Mn site, reducing the likelihood of strong H_2O adsorption that could compete with CO_2 reduction.

The reduction of CO_2 on the Cu site within the Cu-Co paddlewheel complex is expected to be less favorable than on the Co site (Figure S3). This difference primarily arises from several factors, with the foremost being the weaker binding of CO_2 to the Cu site. Additionally, the limiting potential for CO_2 reduction is substantially higher on the Cu site than on the Co site, with values of 1.21 eV and 1.72 eV, respectively. This energy difference of 0.51 eV is larger than that observed for the sites within the Cu-Mn paddlewheel complex (0.61 eV and 1.00 eV for Mn and Cu, respectively). As a result, a higher potential must be applied to initiate CO_2 reduction on the Cu site of the Cu-Co paddlewheel complex, all while competing with the adsorption of CO_2 to the Co site. Hence, our expectation is that the Co site serves as the catalytically active site for the reduction of CO_2 on the Cu-Co paddlewheel complex.

3.5 Cu-Ni Paddlewheel Complex

The adsorption behavior of CO_2 on the individual sites of the Cu-Mn and Cu-Co paddlewheel complexes exhibits significant differences, unlike the Cu-Ni paddlewheel complex, where the difference in binding energy between the Cu and Ni sites is merely 0.10 eV. This smaller energy difference implies that both Cu and Ni sites are likely involved in the CO_2 reduction reaction (Figures 6). Both sites exhibit a preference for reducing CO_2 to $^*OCHO$ rather than $^*OCOH$, with comparable limiting potentials (1.55 eV and 1.37 eV for Cu and Ni, respectively). However, there is a significant disparity in the energy differences between the two reduced intermediates, with values of 0.74 eV for Cu and 0.31 eV for Ni. Moreover, the $^*OCHO$ intermediate is favorably reduced to $^*HCOOH$, following the trends observed for the other complexes.

Slight differences in electronic structures between the two sites becomes more pronounced after the reduction of $^*HCOOH$. On the Ni site (top of Figure 6), the formation of $^*HCO$ is preferred, whereas on the Cu site (bottom of Figure 6), $^*HOCHOH$ formation is favored. Subsequent reductions of $^*HCO$ on the Ni site lead to the formation of $^*CH_2O$, $^*CH_2OH$, and $^*CH_3OH$, ultimately culminating in the production of CH_4. Unlike the Mn and Co sites of their respective paddlewheel complexes, the Ni site does not exhibit strong binding of closed-shell intermediates. The adsorption energies of $^*HCOOH$, $^*CH_2O$, and $^*CH_3OH$ to the Ni site align with those observed in the Cu-Cu paddlewheel complex (Table S1). As a result, the Cu-Ni paddlewheel complex is expected to produce a large proportion of HCOOH, with a smaller amount of CH_4 being produced as well. Additionally, the Ni site is expected to inhibit the coupling of C_1 intermediates and thus, C_2 products are not expected to form.

On the contrary, the Cu site within the Cu-Ni paddlewheel complex is not expected to yield appreciable amounts of CH_4 (bottom of Figure 6). Instead, the favorable reduction of $^*HOCH_2OH$ can occur at either the O or C atoms, resulting in the formation of a free H_2O and an adsorbed $^*CH_2OH$ or free CH_3OH and an adsorbed $^*OH$ intermediate, respectively. The latter reduction is more favorable with a formation energy 0.64 eV lower than the former. This process subsequently leads to the formation of one equivalent each of H_2O and CH_3OH on the Cu site of the Cu-Ni paddlewheel complex.

The binding of $^*HCOOH$ to the Cu site is akin to that on the Ni site and the Cu sites of the Cu-Cu paddlewheel complex, implying that a portion of CO_2 will undergo reduction to form HCOOH as a product. Further reduction of $^*HCOOH$ is expected to lead to CH_3OH production, following the formation of a favorable $^*OH$ intermediate, which hinders the production of CH_4. Anticipated outcomes from CO_2 reduction in the Cu-Ni paddlewheel complex include the production of HCOOH, CH_3OH, and CH_4, with no significant C_2 product formation and only a minor proportion of H_2.

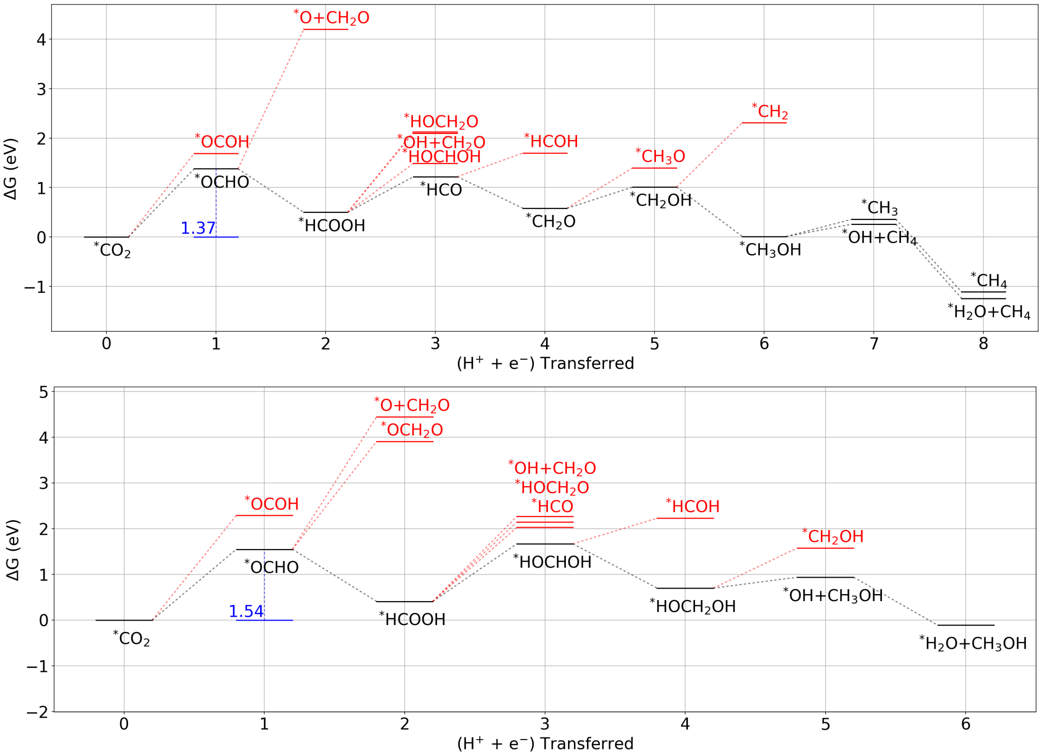

Fig. 6 Free energy reaction mechanism for the reduction of CO_2 on the Ni (top) and Cu (bottom) sites of the Cu-Ni paddlewheel complex. Competing intermediates shown in red. Limiting potential values shown in blue and given in eV.

3.6 Hydrogen Reduction

The hydrogen evolution reaction (HER) often occurs concurrently with and competes against CO_2 reduction, particularly when high voltages are applied. Our investigation reveals that the formation of metal hydrides on the paddlewheel complexes is generally thermodynamically unfavorable, with energy requirements ranging from 0.81 eV to 2.29 eV. An overview of the formation energies linked to these metal hydrides and the subsequent generation of H_2 is presented in Figure 7. Within the array of Cu sites, the incorporation of Mn induces a significant alteration in the metal hydride formation energy, reducing it from 2.29 eV to 1.67 eV. On the contrary, the incorporation of Co or Ni into the paddlewheel complex results in a relatively modest impact on the formation energy, with changes of only 0.08 eV and 0.28 eV, respectively. Nevertheless, the substituent metal itself displays significant variations, with the formation of a Co-hydride being the most energetically favorable at 0.81 eV, while the Mn- and Ni-hydrides require 1.10 eV and 1.67 eV to form, respectively. When functioning solely as a catalyst for hydrogen reduction, the Co-substituted paddlewheel complex exhibits the smallest limiting potential, indicating an expectation for hydrogen reduction with the smallest applied voltage. As a result, the incorporation of substituents into the Cu paddlewheel complexes leads to significantly more favorable hydrogen reduction, potentially influencing the overall efficiency of CO_2 reduction due to the competitive mechanism.

A direct comparison of the limiting potentials for hydrogen and CO_2 reduction provides valuable insights into the competition between these reactions. In Figure 8, the limiting potentials (U_L)

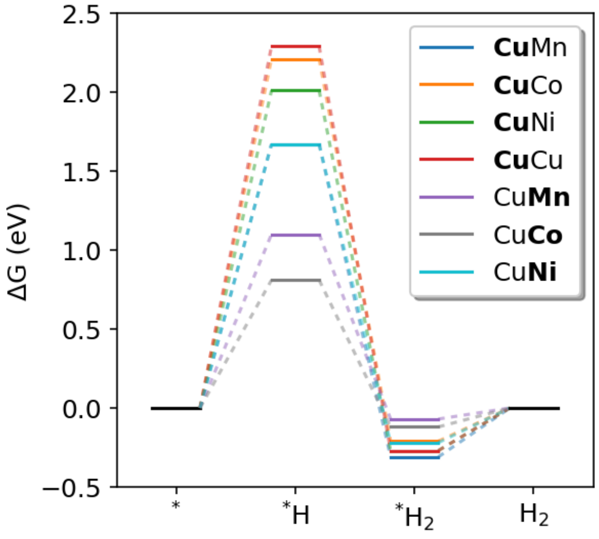

Fig. 7 Free energy reaction mechanism diagram for the reduction of hydrogen to H_2 on the paddlewheel complexes. Values shown in eV. Adsorption sites are highlighted in bold text.

for HER are juxtaposed against those for CO_2RR. Notably, five out of the seven metal sites (those situated in the green region of Figure 8) exhibit more favorable CO_2 reduction, emphasizing their potential in this process. This includes both sites of the Cu-Ni and Cu-Mn complexes and the Cu site of the Cu-Co complex. On the other hand, the Co site within the Cu-Co paddlewheel strongly favors hydrogen reduction. This observation underscores the substantial impact that introducing Co sites into a MOF, such as HKUST-1, could have on CO_2 reduction due to the pronounced competition favoring hydrogen reduction. Finally, the Cu-Cu paddlewheel exhibits nearly identical limiting potential values for HER and CO_2RR. This similarity suggests an anticipated near-equal production of H_2 and reduced CO_2 products, assuming comparable reaction kinetics.

4 Conclusions

The investigation into CO_2 reduction across various mixed-metal paddlewheel complexes has shed light on the profound influence of metal substitution in hetero-bimetallic HKUST-1 materials. Beginning with a comprehensive analysis of the CO_2 reduction reaction in a homo-bimetallic Cu-Cu paddlewheel complex, we gained critical insights into the intricate electronic structure governing the formation of both C_1 and C_2 products, encompassing HCOOH, CO, CH_4, CH_3CH_2OH, C_2H_4, and CH_3COOH. Building upon these foundational insights, our subsequent exploration delved into Cu paddlewheel complexes substituted with Mn(II), Co(II), or Ni(II).

The incorporation of Mn as a metal substituent emerged to be a pivotal enhancement strategy, propelled by the distinctive electronic structure of the Mn site. As a result, there was an inhibition in the production of C_2 products on the Cu site, achieved by strengthening the interactions between the Cu site and open-shell intermediates, thereby discouraging their coupling. Concurrently, it weakened interactions with closed-shell intermediates, leading to a predominant yield of HCOOH from the Cu site and CH_2O from the Mn site. Crucially, the introduction of the Mn site disfavors H_2 production on both sites, thereby enhancing the expected selectivity for CO_2 reduction.

In stark contrast, the Co site within the Cu-Co paddlewheel complex exhibited distinctive catalytic behavior, characterized by stronger CO_2 adsorption and a lower limiting potential for CO_2 reduction compared to the Cu-Cu paddlewheel complex. As a result, this site emerged as the primary catalytic site within the Cu-Co paddlewheel complex, promoting the selective formation of CH_4 through the strong binding of all reduced intermediates. However, the Co site exhibited a lower H_2 limiting potential of 0.81 eV, suggesting that CO_2 reduction would be disfavored due to the higher limiting potential of 1.21 eV on the Co site.

Finally, the Cu-Ni paddlewheel complex unveiled a dual identity, hosting both catalytically active Cu and Ni sites. The Ni site exhibited a tendency for HCOOH and CH_4 formation without significant competition for C_2 product formation, while the Cu site directed the reaction towards HCOOH and CH_3OH production. Additionally, the reduction of hydrogen is disfavored on both the Ni and Cu sites of the Cu-Ni paddlewheel, indicating a lower competition between HER and CO_2RR compared to that observed for HKUST-1.[15]

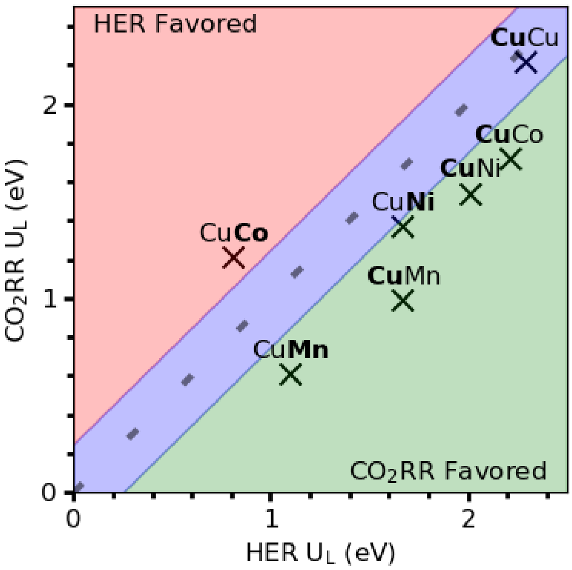

Fig. 8 Limiting potentials for HER and CO_2RR. The red-shaded area represents regions where the U_L values for HER are lower, while the green-shaded area signifies regions with lower U_L values for CO_2RR. The purple-shaded region indicates areas where the U_L values for HER and CO_2RR differ by less than 0.25 eV. Adsorption sites are highlighted in bold text.

The paramount significance of this study lies in its ability to offer essential guidance for experimental chemists, providing invaluable insights for the efficient synthesis and testing of innovative catalysts. The strategic integration of diverse metal substituents into Cu-based paddlewheel complexes emerges as a versatile and potent approach to enhance the CO_2 reduction reaction. These improvements not only mitigate C_2 byproduct formation but also enable precise modulation of selectivity towards C_1 products, encompassing HCOOH, CH_3OH, and CH_4. Moreover, they wield a profound influence on the intricate interplay with hydrogen reduction, thereby molding the catalytic landscape for CO_2 reduction across a diverse array of applications.

Author Contributions

G.A.M.: conceptualization, data curation, formal analysis, investigation, methodology, software, validation, visualization, writing - original draft, writing - review & editing. T.Y. and W.Z.: project administration, resources, supervision.

Conflicts of interest

There are no conflicts to declare.

Acknowledgements

G.A.M would like to thank NIST's Postdoctoral Program for an NRC Postdoctoral Fellowship.

References

1 J. S. Sperry, M. D. Venturas, H. N. Todd, A. T. Trugman, W. R. L. Anderegg, Y. Wang and X. Tai, *Proceedings of the Na-*

tional Academy of Sciences, 2019, **116**, 25734–25744.

2 M. W. Jones, G. P. Peters, T. Gasser, R. M. Andrew, C. Schwingshackl, J. Gütschow, R. A. Houghton, P. Friedlingstein, J. Pongratz and C. Le Quéré, *Scientific Data*, 2023, **10**, 155.

3 M. He, S. Piao, C. Huntingford, H. Xu, X. Wang, A. Bastos, J. Cui and T. Gasser, *Communications Earth & Environment*, 2022, **3**, 160.

4 J. G. Vitillo, B. Smit and L. Gagliardi, *Chemical Reviews*, 2017, **117**, 9521–9523.

5 M. Yousaf, M. Zaman, A. Mahmood, M. Imran, A. Elkamel, M. Rizwan, T. Wilberforce and F. Riaz, *Energy Science & Engineering*, 2022, **10**, 4890–4923.

6 Y. Jiang, T.-d. Hu, L.-y. Yu and Y.-h. Ding, *Nanoscale Advances*, 2021, **3**, 4079–4088.

7 L. Cui, C. Liu, B. Yao, P. P. Edwards, T. Xiao and F. Cao, *Frontiers in Chemistry*, 2022, **10**, year.

8 W. Li, H. Wang, X. Jiang, J. Zhu, Z. Liu, X. Guo and C. Song, *RSC Advances*, 2018, **8**, 7651–7669.

9 R. Francke, B. Schille and M. Roemelt, *Chemical Reviews*, 2018, **118**, 4631–4701.

10 V. Kumaravel, J. Bartlett and S. C. Pillai, *ACS Energy Letters*, 2020, **5**, 486–519.

11 S. Nitopi, E. Bertheussen, S. B. Scott, X. Liu, A. K. Engstfeld, S. Horch, B. Seger, I. E. L. Stephens, K. Chan, C. Hahn, J. K. Nørskov, T. F. Jaramillo and I. Chorkendorff, *Chemical Reviews*, 2019, **119**, 7610–7672.

12 K. P. Kuhl, E. R. Cave, D. N. Abram and T. F. Jaramillo, *Energy Environ. Sci.*, 2012, **5**, 7050–7059.

13 W.-G. Cui, G.-Y. Zhang, T.-L. Hu and X.-H. Bu, *Coordination Chemistry Reviews*, 20419, **387**, 79–120.

14 Z. Weng, Y. Wu, M. Wang, J. Jiang, K. Yang, S. Huo, X.-F. Wang, Q. Ma, G. W. Brudvig, V. S. Batista, Y. Liang, Z. Feng and H. Wang, *Nature Communications*, 2018, **9**, 415.

15 D.-H. Nam, O. S. Bushuyev, J. Li, P. De Luna, A. Seifitokaldani, C.-T. Dinh, F. P. García de Arquer, Y. Wang, Z. Liang, A. H. Proppe, C. S. Tan, P. Todorović, O. Shekhah, C. M. Gabardo, J. W. Jo, J. Choi, M.-J. Choi, S.-W. Baek, J. Kim, D. Sinton, S. O. Kelley, M. Eddaoudi and E. H. Sargent, *Journal of the American Chemical Society*, 2018, **140**, 11378–11386.

16 M. Perfecto-Irigaray, J. Albo, G. Beobide, O. Castillo, A. Irabien and S. Pérez-Yáñez, *RSC Advances*, 2018, **8**, 21092–21099.

17 T. Van Phuc, S. G. Kang, J. S. Chung and S. H. Hur, *Materials Research Bulletin*, 2021, **138**, 111228.

18 I. Choi, Y. E. Jung, S. J. Yoo, J. Y. Kim, H.-J. Kim, C. Y. Lee and J. H. Jang, *Journal of Electrochemical Science and Technology*, 2017, **8**, 61–68.

19 G. A. McCarver, T. Yildirim and W. Zhou, *ChemPhysChem*, 2023, **24**, e202300645.

20 D. Narváez-Celada and A. S. Varela, *J. Mater. Chem. A*, 2022, **10**, 5899–5917.

21 X. Kang, Q. Zhu, X. Sun, J. Hu, J. Zhang, Z. Liu and B. Han, *Chemical Science*, 2016, **7**, 266–273.

22 R. Senthil Kumar, S. Senthil Kumar and M. Anbu Kulandainathan, *Electrochemistry Communications*, 2012, **25**, 70–73.

23 C. Wang, Z. Lv, W. Yang, X. Feng and B. Wang, *Chemical Society Reviews*, 2023, **52**, 1382–1427.

24 D. T. Wijaya and C. W. Lee, *Chemical Engineering Journal*, 2022, **446**, 137311.

25 K. Świrk, G. Delahay, A. Zaki, K. Adil and A. Cadiau, *ChemCatChem*, 2021, **13**, 4029–4037.

26 J. M. Veleta, R. A. Arrieta, Y. Wu, M. A. Baeza, K. Castañeda and D. Villagrán, *Langmuir*, 2023, **39**, 8091–8099.

27 N. K. Gupta, J. Bae and K.-S. Kim, *Materials*, 2022, **15**, 2804.

28 D. M. Shakya, O. A. Ejegbavwo, T. Rajeshkumar, S. D. Senanayake, A. J. Brandt, S. Farzandh, N. Acharya, A. M. Ebrahim, A. I. Frenkel, N. Rui, G. L. Tate, J. R. Monnier, K. D. Vogiatzis, N. B. Shustova and D. A. Chen, *Angewandte Chemie International Edition*, 2019, **58**, 16533–16537.

29 A. J. Brandt, D. M. Shakya, K. Metavarayuth, E. Dolgopolova, L. Hensley, A. S. Duke, S. Farzandh, M. Stefik, N. B. Shustova and D. A. Chen, *Langmuir*, 2020, **36**, 9900–9908.

30 I. Jahan, M. Amirul Islam, T. Hasan Rupam, M. L. Palash and B. Baran Saha, *Thermal Science and Engineering Progress*, 2022, **35**, 101453.

31 J. M. Veleta, R. A. Arrieta, Y. Wu, M. A. Baeza, K. Castañeda and D. Villagrán, *Langmuir*, 2023, **39**, 8091–8099.

32 T.-d. Hu, Y. Jiang and Y.-h. Ding, *Journal of Materials Chemistry A*, 2019, **7**, 14825–14834.

33 K. Metavarayuth, O. Ejegbavwo, G. McCarver, M. Myrick, T. Makris, K. Vogiatzis, S. Senanayake, O. Manley, A. Ebrahim, A. Frenkel, S. Hwang, T. Rajeshkumar, J. Jimenez, K. Chen, N. Shustova and D. Chen, *Journal of Physical Chemistry Letters*, 2020, **11**, 8138–8144.

34 D. Chen, J. Jimenez, S. Senanayake, J. Stetzler, D. Shakya, G. Mccarver, T. Rajeshkumar, K. Vogiatzis, A. Mathur, N. Shustova, M. Myrick, K. Metavarayuth, M. Royko, J. Lauterbach, G. Tate and J. Monnier, *Journal of Physical Chemistry C*, 2022, **126**, year.

35 Y. Zhao and D. G. Truhlar, *The Journal of Chemical Physics*, 2006, **125**, 194101.

36 F. Neese, F. Wennmohs, U. Becker and C. Riplinger, *The Journal of Chemical Physics*, 2020, **152**, 224108.

37 F. Weigend, *Physical Chemistry Chemical Physics*, 2006, **8**, 1057–1065.

38 J. Kalinowski, F. Wennmohs and F. Neese, *Journal of Chemical Theory and Computation*, 2017, **13**, 3160–3170.

39 F. Weigend and R. Ahlrichs, *Physical Chemistry Chemical Physics*, 2005, **7**, 3297.

40 S. Grimme, J. Antony, S. Ehrlich and H. Krieg, *The Journal of Chemical Physics*, 2010, **132**, 154104.

41 S. Grimme, *Chemistry – A European Journal*, 2012, **18**, 9955–9964.

42 V. Barone and M. Cossi, *The Journal of Physical Chemistry A*, 1998, **102**, 1995–2001.

43 D. R. Weinberg, C. J. Gagliardi, J. F. Hull, C. F. Murphy, C. A. Kent, B. C. Westlake, A. Paul, D. H. Ess, D. G. McCafferty and

T. J. Meyer, *Chemical Reviews*, 2012, **112**, 4016–4093.

44 R. Tyburski, T. Liu, S. D. Glover and L. Hammarström, *Journal of the American Chemical Society*, 2021, **143**, 560–576.

45 A. A. Peterson, F. Abild-Pedersen, F. Studt, J. Rossmeisl and J. K. Nørskov, *Energy and Environmental Science*, 2010, **3**, 1311–1315.

46 C. H. Hendon and A. Walsh, *Chemical Science*, 2015, **6**, 3674–3683.